Assessing direction-specific adaptation using the steady-state visual evoked potential: Results from EEG source imaging

Justin M. Ales

Smith-Kettlewell Eye Research Institute, San Francisco, CA, USA

Anthony M. Norcia

Smith-Kettlewell Eye Research Institute, San Francisco, CA, USA

Studying directional selectivity using neuroimaging in humans is difficult because the resolution is insufficient to directly access directionally selective activity. Here we used motion adaptation of the steady-state visual evoked potential (SSVEP) and source imaging in the frequency domain to detect brain areas that contain direction-selective cells. This study uses a definitive electrophysiological marker for direction-specific adaptation in the SSVEP to localize cortical areas that are direction selective. It has been shown previously that an oscillating stimulus produces an SSVEP response that is dominated by even harmonics of the stimulus frequency. This pattern of response is consistent with equal population responses to each direction of motion. Prolonged exposure to unidirectional motion induces an asymmetry in the population response that is consistent with adaptation of direction-selective cells. This asymmetry manifests itself in the presence of odd harmonic components after adaptation Critically, the feature that indicates the direction used for adaptation is the phase of the odd-harmonic responses. We recorded this signature of direction selectivity in a group of observers whose retinotopic visual areas had been defined from fMRI mapping. We find direction-specific responses throughout retinotopic cortex, with the largest effect in areas V1 (occipital pole) and V3/V3a (dorsal).

Keywords: SSVEP, motion, adaptation, source localization, fMRI, direction selectivity

Citation: Ales, J. M., & Norcia, A. M. (2009). Assessing direction-specific adaptation using the steady-state visual evoked potential: Results from EEG source imaging. *Journal of Vision, 9*(7):8, 1–13, http://journalofvision.org/9/7/8/, doi:10.1167/9.7.8.

Introduction

Individual neurons in many cortical areas are direction selective (Albright, 1984; Felleman & Van Essen, 1987; Orban, Kennedy, & Bullier, 1986). Studying the activity of direction-specific neurons in humans necessitates the use of noninvasive measures such as the EEG/MEG or fMRI. Direction selectivity is not directly apparent in these mass responses, however, because cortical areas containing neurons that are selective for direction of motion will respond equally—at the population level—for a stimulus moving in any direction. Moreover, it is not immediately obvious with these measures that any or all of the evoked response associated with a moving stimulus derives from direction-selective neurons because responses could be evoked from mechanisms that respond simply to local luminance or contrast transients.

There have been numerous previous studies that have recorded M/EEG responses to moving stimuli and performed source localization to determine the cortical locus of the evoked responses. Many of these studies recorded responses that occurred at the transition between moving and static targets (Bundo et al., 2000; Prieto et al., 2007; Probst, Plendl, Paulus, Wist, & Scherg, 1993; Schellart, Trindade, Reits, Verbunt, & Spekreijse, 2004; von Pfostl et al., 2009). All of these studies have found sources of activity in occipital, temporal–occipital, and occipital–parietal cortex. The response to the onset of a motion from a static period contains responses to the motion, but also to the nonmotion, or "flicker," transients in the stimulus. To avoid this confound, several authors have used stimuli that transition from incoherently moving dots to coherent motion (Handel, Lutzenberger, Thier, & Haarmeier, 2007; Holliday & Meese, 2008; Lam et al., 2000; Nakamura et al., 2003). Differential responses to incoherent and coherent motion require the existence of direction-selective units, but these paradigms subtract out the common responses to local motion. All of the studies that have used stimuli that transition from incoherent to coherent motion have found activity in temporal–occipital cortex that modulates with onset of coherent motion. Handel et al. (2007) found an additional source in the occipital region. Two other studies localized responses to higher levels of motion processing, by contrasting responses to expansion, contraction, rotation, and translation (Delon-Martin et al., 2006; Holliday & Meese, 2008). These stimuli are isolate response mechanisms that

doi: 10.1167/9.7.8 Received January 22, 2009; published July 14, 2009 ISSN 1534-7362 © ARVO

can distinguish between optic flow components. Both of these studies found responses in throughout occipital, temporal–occipital, and occipital–parietal cortex and found that different regions differentiated between classes of global motion. The studies that contrast global motion organizations also subtract out the common local motion responses, making them insensitive brain areas that respond only to local motion. One previous source localization study retained sensitivity to even local motion responses by using direction-specific adaptation (Amano, Kuriki, & Takeda, 2005). MEG responses were about a factor of 2 lower in amplitude following same-direction adaptation. Dipole fitting found sources at the occipital pole/calcarine sulcus in temporal–occipital cortex.

A common method used to reveal human directional mechanisms is selective adaptation. Direction-specific adaptation has been used widely in psychophysical studies to infer tuning properties of directional mechanisms in humans (Nishida, Ledgeway, & Edwards, 1997; Schor & Levi, 1980; Sekuler & Ganz, 1963; Steiner, Blake, & Rose, 1994), and direction-specific adaptation has also been used with the visual evoked potential (VEP) to study human motion mechanisms (Heinrich & Bach, 2003; Hoffmann, Unsold, & Bach, 2001; Tyler & Kaitz, 1977). Adaptation has also be used with fMRI (Ashida, Lingnau, Wall, & Smith, 2007; Huk, Ress, & Heeger, 2001; Nishida, Sasaki, Murakami, Watanabe, & Tootell, 2003). Each of these methods infers direction selectivity by measuring responses to a test stimulus before and after adaptation.

Prior VEP studies have found a large effect of unidirectional motion adaptation on the responses in both the transient (Heinrich & Bach, 2003; Hoffmann et al., 2001) and steady-state response (Heinrich & Bach, 2003; Tyler & Kaitz, 1977). VEP adaptation effects may arise as a result of specific adaptation to direction of motion or to a more general adaptation to contrast/flicker. Hoffman et al. (2001) used an unadapted control along with several adapter directions to study direction tuning. The directionally specific component was quantified as the additional adaptation, as compared with the unadapted control, induced by the change in adapter direction. Heinrich and Bach (2003) added a nondirectional oscillatory adapter condition that factored out nonspecific contrast adaptation effects. Tyler and Kaitz (1977) reasoned that direction-specific adaptation should render the normally symmetric oscillatory motion response asymmetric, with the result being the production of odd harmonic responses. Indeed, they found that prior to adaptation, the response to an oscillating grating contained only even harmonics of the stimulus frequency, but after adaptation a strong first harmonic was present. Our method extends the frequency domain analysis of Tyler and Kaitz by using an additional criterion for direction-specific adaptation: the phase of the induced first harmonic must be opposite for opposite direction adapters.

All previous VEP studies have used a small number of electrodes, precluding an assessment of the possible cortical loci of the measured adaptation effects. We used a distributed source reconstruction method to study direction-specific adaptation across a series of cortical regions of interest (ROIs) determined by functional and retinotopic fMRI mapping. This method allows us to compare the location of the adaptation effects seen in our data to previous fMRI studies of motion adaptation (Ashida et al., 2007; Huk et al., 2001; Nishida et al., 2003).

Methods

Participants

A total of seven observers participated (four male, mean age = 43.7 years). All participants had visual acuity of 20/20 or better in each eye, with correction if needed, and stereoacuity of 40 arc seconds or better on the Titmus and Randot stereoacuity tests. Acuity was measured using the Bailey–Lovie chart, which has five letters per line and equal log increments in the letter sizes across lines. Informed consent was obtained prior to experimentation under a protocol that was approved by the institutional review board of the Smith-Kettlewell Eye Research Institute.

Stimulus generation

Stimulus generation and signal analysis were performed by in-house software, running on a Macintosh G4 platform. Stimuli were presented in a dark and quiet room on a LaCie electron19blueIV (Model N2901) monitor at a resolution of 800 × 600 pixels, with a 72-Hz vertical refresh rate. The nonlinear voltage versus luminance response of the monitor was corrected in software after calibration of the display with an in-house linear PIN-diode photometer equipped with a photopic filter.

The adapting stimulus consisted of a 2 cycle per degree vertical sinusoidal grating presented at 80% contrast and viewed from 100 cm (width of 20 degrees, height of 15 degrees). The drifting adapting stimulus (4.5 deg/s) was viewed for 25.6 seconds. Immediately after the adaptation the test stimulus was displayed and oscillated at 9 Hz through 15 minutes of arc for 10.00 seconds. The test–stimulus oscillation had a temporal square-wave profile that led to an equivalent velocity of 2.25 deg/s.

Adaptation procedure

A session began with a block of 10 test trials (unadapted) that was followed by 10 trials of a randomly chosen left or right adaptation/test cycle. The adaptation/

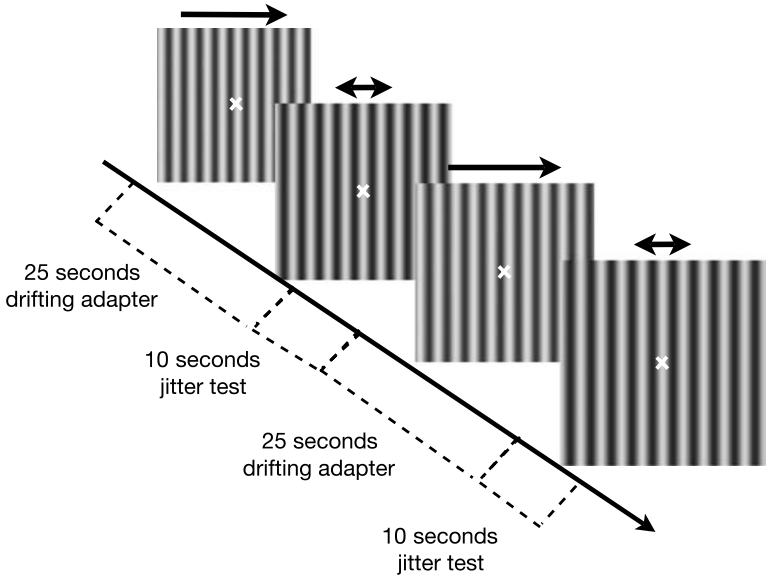

Figure 1. Schematic diagram of the temporal sequence of the adaptation blocks. The unidirectional adaptor was presented for 25.6 seconds followed immediately by 10.0 seconds of the test condition. A block consisted of 10 repeats of this cycle. Leftward and rightward adaptation blocks were presented.

test cycle within a block is illustrated in Figure 1. After an adaptation block, the participant was allowed to rest for several minutes in order to dissipate the adaptation effect. At this point, another block of 10 trials of the oscillating test grating was presented without adaptation. This test phase was followed by an adaptation/test block in which the, the direction of the adaptor was the reverse of that presented in the first adaptation block. This block was followed by several minutes of rest, after which a final block of 10 trials of the oscillating test grating was presented. The multiple oscillating test blocks were used to control for possible time-dependent effects over the duration of the recording. Participants were instructed to fixate a cross at the center of the display and to distribute attention evenly over the entire display during both test and adapt phases.

Spectral signature of direction-specific adaptation

In order to understand how our analysis reveals directionally specific adaptation, simulated and actual responses are shown in Figure 2. The first row of Figure 2 illustrates an input that oscillates back and forth. The next row shows hypothetical responses of a population of directionally selective cells. The response of each population is rendered as half wave-rectified sine wave at the fundamental of the square wave input. The responses for rightward selective cells are shown in red and the leftward population response is shown in blue. In the unadapted state, both populations respond equally well to each direction. The summed population response at the scalp is a full wave rectified version of the input. This rectification results in a frequency doubling of the response, but this frequency doubling is not diagnostic of directional selectivity. Frequency doubling can also result from individual neuron responses that are not direction selective. In order to reveal the directionally selective responses, we will use adaptation to a single direction. After adaptation to a specific direction of motion, the responses of individual neurons from the population that are directionally selective will be reduced, resulting in an imbalance in the overall response to the oscillating stimulus. In the example, the unadapted response has six equal responses to three cycles of the input, an even multiple of the input frequency. In contrast, the example-adapted case exhibits an odd multiple of the input frequency, three strong and three weak responses. There is an additional feature in the bottom two rows that differentiates the direction used to adapt. The imbalanced-adapted response has a different temporal sequence, either strong/weak or weak/strong, depending on the direction of the adapting stimulus. The different temporal ordering results in a 180-degree phase difference in odd harmonic components. The presence of odd harmonics that are 180-degree phase shifted after adapting to different directions of motion is a strong diagnostic check for the presence of directional selectivity. The simulated effects on the left side of Figure 2 can be seen in real data plotted in the phasor diagrams on the right.

EEG signal acquisition and source imaging procedure

The EEG signal acquisition, head conductivity modeling, source estimation, visual area definition, and

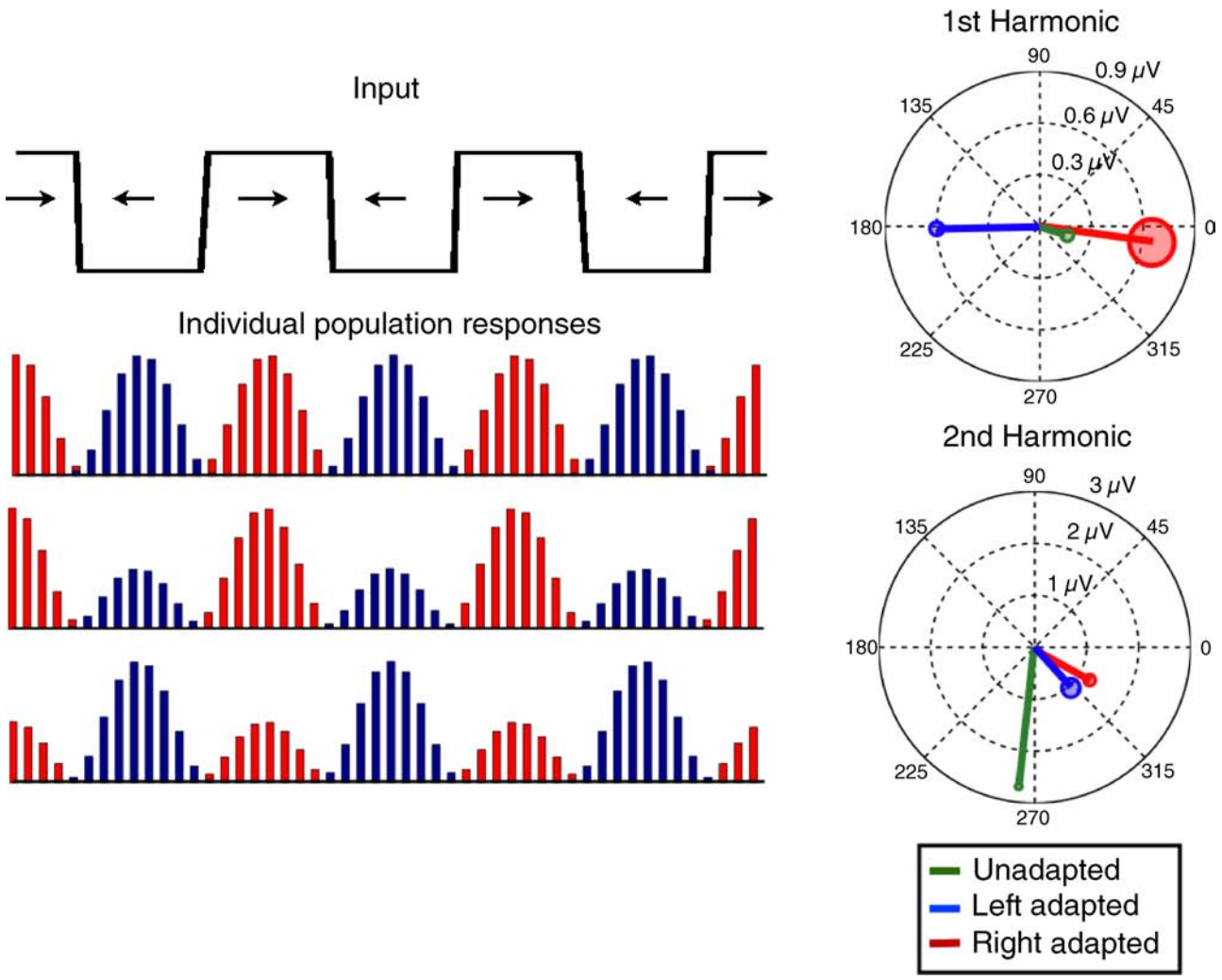

Figure 2. An example of our data analysis. The top left shows the temporal sequence of the right and left movements of a steady-state oscillating stimulus. Below that are simulated post stimulus time histograms of the hypothetical responses of directional-selective neurons (red bars for right selective, and blue bars for left selective). The top histogram shows responses prior to any adaptation both cells responds equally. The middle histogram shows responses after adapting to a leftward stimulus; in this case, the left selective cells have a reduced response, while the bottom histogram shows the right selective cells being adapted. On the right side of this figure are SSVEP data from an occipital pole electrode. The top plot is the first harmonic phasor, and the bottom plot is the second harmonic phasor. Green shows unadapted responses, and blue and red are after leftward or rightward adaptation.

region-of-interest (ROI) quantification are similar to those described in Appelbaum, Wade, Vildavski, Pettet, and Norcia (2006). In the interest of brevity, we will only provide an overview of these methods here, highlighting differences in procedure, as appropriate.

The electroencephalogram (EEG) was collected with 128-sensor HydroCell Sensor Nets (Electrical Geodesics, Eugene, OR). The EEG was amplified at a gain of 1,000 and recorded with a vertex physical reference. Signals were 0.1 Hz high-pass and 50 Hz (elliptical) low-pass filtered and digitized at 432 Hz with a precision of 4 bits per microvolt at the input. Following each experimental session, the 3D locations of all electrodes and three major fiducials (nasion, left, and right peri-auricular points) were digitized using a 3Space Fastrack 3D digitizer (Polhemus, Colchester, VT). For all observers, the 3D digitized locations were used to coregister the electrodes to their T1-weighted anatomical magnetic resonance (MR) scans.

Artifact rejection and spectral analysis of the EEG data were done off-line. Raw data were evaluated according to a sample-by-sample thresholding procedure to remove noisy sensors that were replaced by the average of the six nearest spatial neighbors. Once noisy sensors were substituted, the EEG was re-referenced to the common average of all the sensors. Additionally, EEG epochs that contained a large percentage of data samples exceeding threshold (~40–80 μV) were excluded on a sensor-by-sensor basis. Time averages for each stimulus condition were computed over one stimulus cycle (111 ms). To avoid onset effects, the first 1 second was excluded from

analysis. The time averages were then converted to complex-valued amplitude spectra at a frequency resolution of 0.5 Hz via a discrete Fourier transform. The resulting amplitude spectra of the steady-state visual evoked potential (SSVEP) were then evaluated at all harmonics of the frequencies of the input stimulus frequency tag. Significance was assessed using the $Tcirc^2$ statistic (Victor & Mast, 1991).

Head conductivity and geometry models

As part of the source-estimation procedure, bound element method (BEM) head tissue conductivity models were derived from T1- and T2-weighted MRI scans of each observer (Siemens Trio 3T, 1 mm isotropic resolution). The FSL toolbox was used to segment contiguous volume regions for the scalp, outer skull, inner skull, and the cortex and to convert these MRI volumes into inner skull, outer skull, and scalp surfaces (Smith, 2002; Smith et al., 2004; Jenkinson, Pechaud, & Smith, 2005). The boundary element equations were computed from these surfaces using the MNE Suite (Hamalainen & Sarvas, 1989).

The FreeSurfer software package (http://surfer.nmr.mgh.harvard.edu) was used to perform gray and white matter segmentation and a mid-gray cortical surface extraction for use with the cortically constrained minimum norm inverse. The FreeSurfer package extracts both gray/white and gray/cerebrospinal fluid (CSF) boundaries, but these surfaces can have different surface orientations. In particular, the gray/white boundary has sharp gyri (the curvature changes rapidly) and smooth sulci (slowly changing surface curvature), while the gray/CSF boundary is the inverse, with smooth gyri and sharp sulci. In order to avoid these discontinuities, we generated a surface partway between these two boundaries that has gyri and sulci with approximately equal curvature. Sources were constrained to lie on this surface with their orientation constrained to the local surface normal. Coregistration of the electrode positions to the MRI head surface was done in MATLAB by a least-squares fit of the three digitized fiducial points to their visible locations on the anatomical MRI.

Cortically constrained minimum norm source estimates

Estimates of the underlying cortical activity were derived using a cortically constrained minimum norm implemented in Matlab.

$$D = FX + \sigma, \tag{1}$$

$$X = (F^t F)^{-1}(F^t D). \tag{2}$$

Equation 1 is our model of the system. The matrix D is the recorded data, with dimensions of electrodes (128) by time points (48). The matrix F is the forward model, whose dimensions are electrodes (128) by sources (20,428). F maps every vertex on the cortex to a voltage on the scalp electrodes. The matrix X is the quantity we are estimating, it is the source temporal response matrix, with dimensions of sources (20,484) by time points (48). The matrices in Equation 1 are illustrated graphically in Figure 3. The images in Figure 3 were taken from data used in this experiment. The model is based on the assumption that surface EEG signals are generated by multiple dipolar sources located in the gray matter and oriented perpendicular to the cortical surface. Calculation of the inverse of F was accomplished through a singular value decomposition (SVD) inversion. Regularization of the SVD inversion was done by truncating any singular values of the inverse matrix that had a condition number of less than 100. The results are robust to the choice of this parameter, we have tried various condition numbers, from 10 to 500, and the results are similar. This solution is equivalent to solving the following optimization.

$$\underset{X}{\operatorname{argmin}} \left(\|D - FX\|_F^2 + \lambda \|X\|_F^2 \right). \tag{3}$$

The first term of the quantity to be minimized in Equation 3 is the goodness of fit or how well the model (FX, the sources projected through the forward matrix) fits the data (D). Because there are more sources than electrodes, the problem is ill posed and there are many solutions that fit the data. Therefore, an additional term is needed to provide a unique solution. The second half of the equation quantifies the "goodness" of the model parameters (X).

The classical choice for quantifying the model parameter goodness is the minimum L2-norm solution (Hamalainen & Ilmoniemi, 1994), the solution with the minimum sum square voltage. Since this cost function penalizes the squares of the voltages, large values are abhorred, i.e., two nearby sources would each rather share the load with each receiving half the amplitude. From the Bayesian inference perspective, the L2 norm is identical to assuming a Gaussian prior on source amplitudes. This prior explains why large amplitudes are so heavily penalized; the large values lie far out on the tails of the Gaussian and hence have a low probability. The regularization parameter λ adjusts the trade off between fitting the data well and matching the prior. Larger values of λ allow greater misfits to the data and enforce a better fit to the prior.

Visual area definition by fMRI functional and retinotopic mapping

In order to avoid inaccuracies associated with individual differences in cortical geometry with respect to the sensors

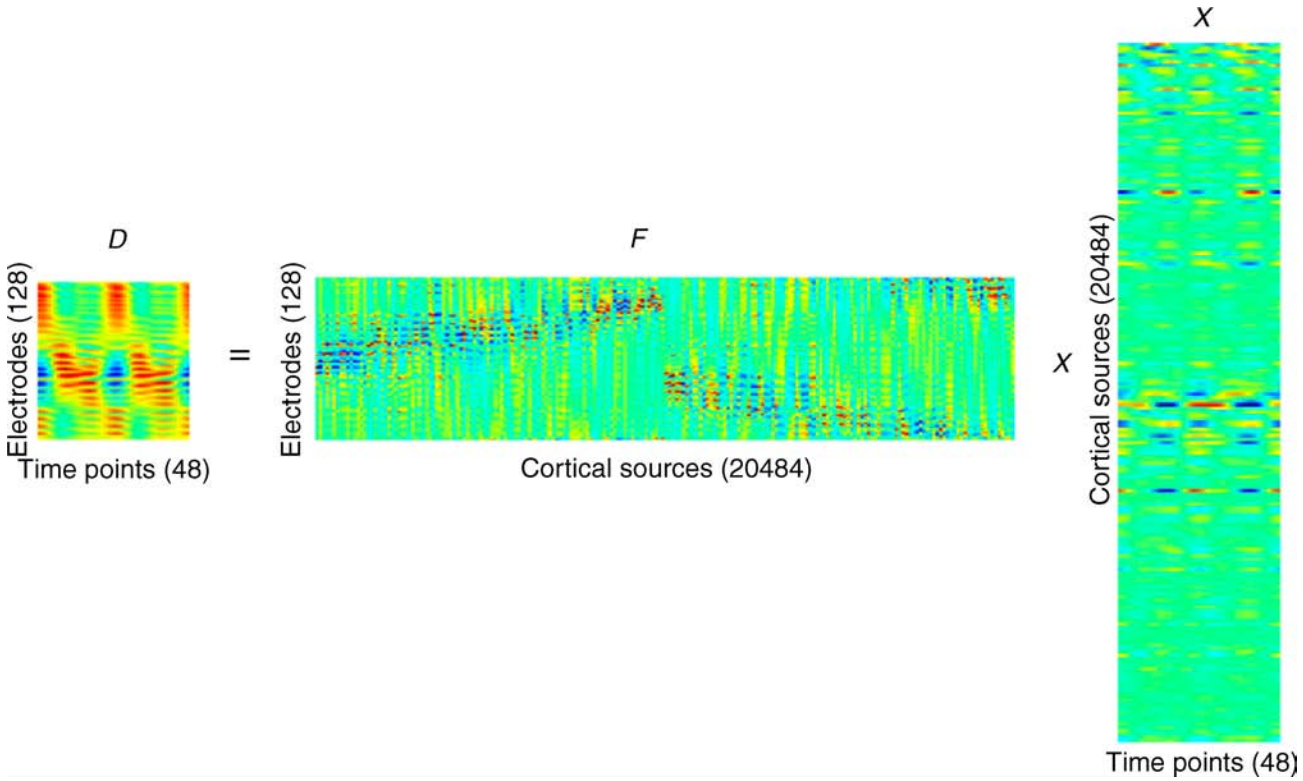

Figure 3. Graphical representation of the linear algebra matrices used for Equation 1. The matrix images are the data used in the analysis.

and the precise location of visual areas with respect to gyri and sulci, we extracted evoked response data from CCD distributions that lay within specific retinotopically or functionally defined ROIs on a participant-by-participant basis.

For all observers, functional magnetic resonance imaging (fMRI) scans were collected on a Siemens Trio 3T scanner, the voxel size was 1.7 × 1.7 × 2 mm with a field of view of 220 × 220 × 60 mm. The general procedures for these scans (head stabilization, visual display system, etc.) are standard and have been described in detail elsewhere (Brewer, Liu, Wade, & Wandell, 2005; Tyler et al., 2005). Retinotopic field mapping produced ROIs defined for each participant's visual cortical areas V1, V2v, V2d, V3v, V3d, V3A, and V4 in each hemisphere (DeYoe et al., 1996; Tootell & Hadjikhani, 2001; Wade, Brewer, Rieger, & Wandell, 2002). ROIs corresponding to each participant's hMT+ were identified using low contrast motion stimuli similar to those described by Huk and Heeger (2002).

The lateral occipital complex (LOC) was defined using a block-design fMRI localizer scan. During this scan, the observers viewed blocks of images depicting common objects (18 seconds/block) alternating with blocks containing scrambled versions of the same objects. The stimuli were those used in a previous study (Kourtzi & Kanwisher, 2000). The regions activated by these scans included an area lying between the V1/V2/V3 foveal confluence and hMT+ that we identified as LOC. Retinotopic visual areas and area hMT+ bound the LOC.

Region-of-interest (ROI) response quantification

An estimate of the frequency-tagged response for each ROI was computed by averaging responses across its vertices. This was done by first applying the above-described minimum L2-norm inverse to the complex valued frequency domain data. This gives a complex valued result at every vertex (node) on the cortical surface. Next, a single complex-valued component was computed for each ROI by averaging across all nodes within that ROI across both hemispheres. This averaging was performed on the complex Fourier components and therefore preserved phase information.

Results

As noted above, the signature of direction-specific adaptation is the production of odd harmonic responses that are 180 degrees out of phase after opposite directions of adaptation. A phasor diagram of the data recorded from a single participant at an electrode located near the occipital pole illustrates the adaptation effect (see Figure 2). The response recorded at the first harmonic prior to adaptation (shown in green) increases several fold after adaptation and is highly significant

(shown in red and blue). The increase in response strength at the first harmonic is the same for both directions of adaptation, but the response phase differs by 180 degrees for the two adaptor directions. The second harmonic in this participant is reduced in amplitude after adaptation and is also shifted in phase by about 45 degrees in the lag direction, but this was not characteristic of the group, as a whole.

Scalp topography

Figure 4 shows the scalp distribution of a single participant for the first and second harmonics, both before and after adaptation. Response amplitude is coded according to the color bar. Both first and second harmonics are maximal at occipital electrodes. The leftmost plot in the first row of Figure 4 shows that the first harmonic response is small prior to adaptation. The next two plots in the first row show that after adaptation, however, the first harmonic is significantly larger. For this participant, the second harmonic responses in the bottom row are somewhat smaller after adaptation, but the response topographies have a comparable shape across conditions. The reduction in amplitude is not seen in the group average shown in Figure 5. The group average shows that the first harmonic response amplitude is small prior to adaptation and is larger after adaptation (see first row). The second harmonic amplitudes are comparable across conditions (second row).

Source distribution

The underlying sources of the direction-specific first-harmonic responses and the nonspecific second harmonics were reconstructed using the L2 norm. Source reconstructions for the participant shown in Figure 4 are shown in Figure 6. For the nonadapted condition, there is a large response at the second harmonic nd no response that is above the plotting threshold at the first harmonic. After adaptation, the first harmonic shows an increase of response around the occipital pole. The source distribution of the second harmonic remains largely unchanged after adaptation.

The cortical current density reconstructions provide a nice qualitative rendering of the data; however, it is hard to draw quantitative conclusions from them and it is difficult to simultaneously view amplitude and phase data. We are also interested in determining the degree to which different cortical areas are adapted. To demonstrate the presence of the direction-specific adaptation signature within our visual ROIs, we plotted group average phasor diagrams of the first harmonic in three visual ROI's Figure 7. shows that the first harmonic increases after adaptation and that each area shown displays the signature for directionally specific cells.

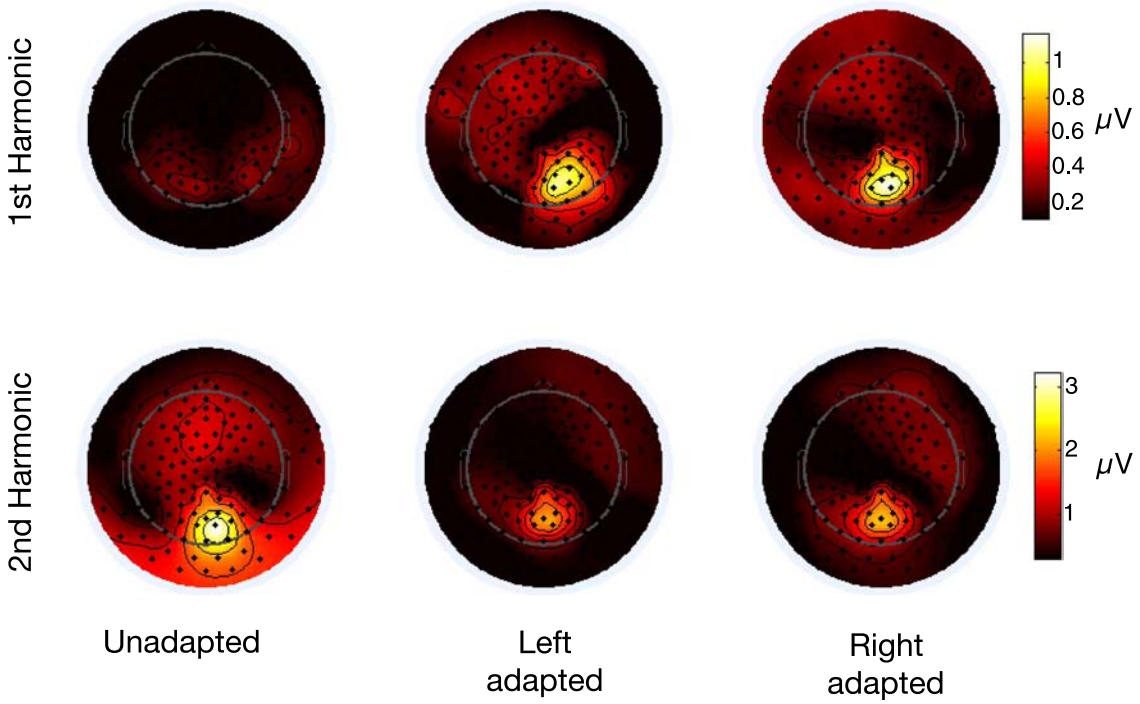

Figure 4. Scalp topographies from a single participant. The top row shows the responses at the first harmonic; the bottom row shows the second harmonic responses. Note that within a row the scale is consistent, but that each row is scaled differently. The leftmost column is from the unadapted trials, the middle column shows data after adaptation to leftward drift, and the rightmost column after a rightward drift.

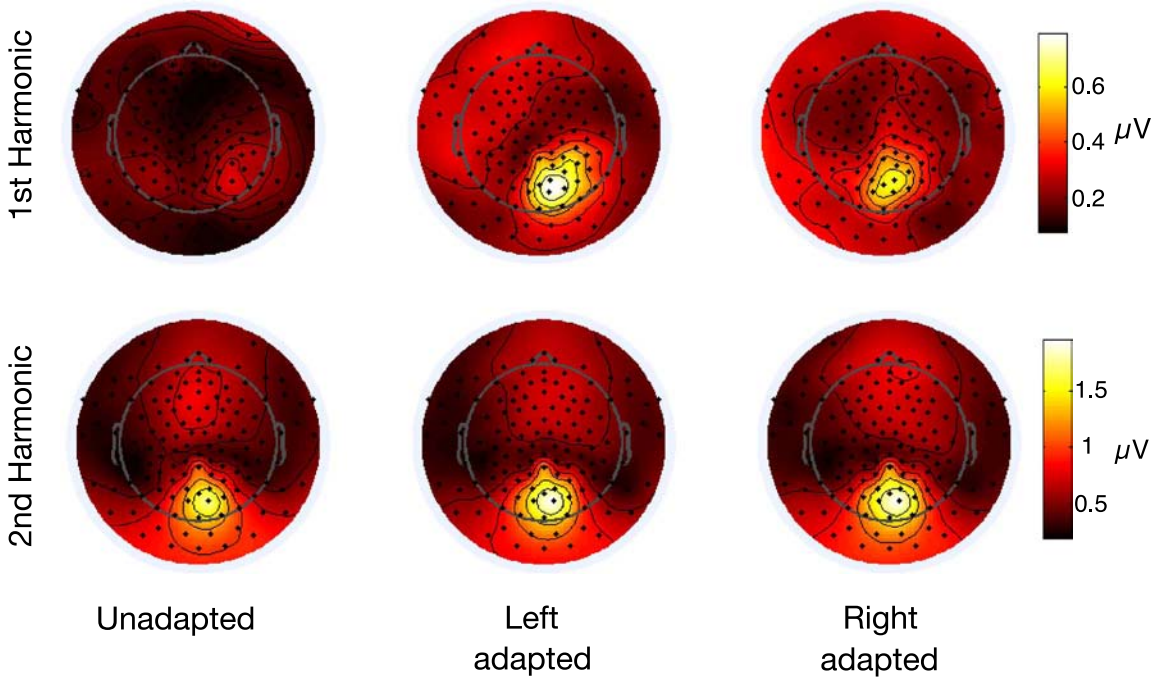

Figure 5. Scalp topographies averaged over all participants. The top row shows the responses at the first harmonic, the bottom row shows the second harmonic responses. Note that within a row, the scale is consistent, but that each row is scaled differently. The leftmost column is from the unadapted trials, the middle column shows data after adaptation to leftward drift, and the rightmost column after a rightward drift.

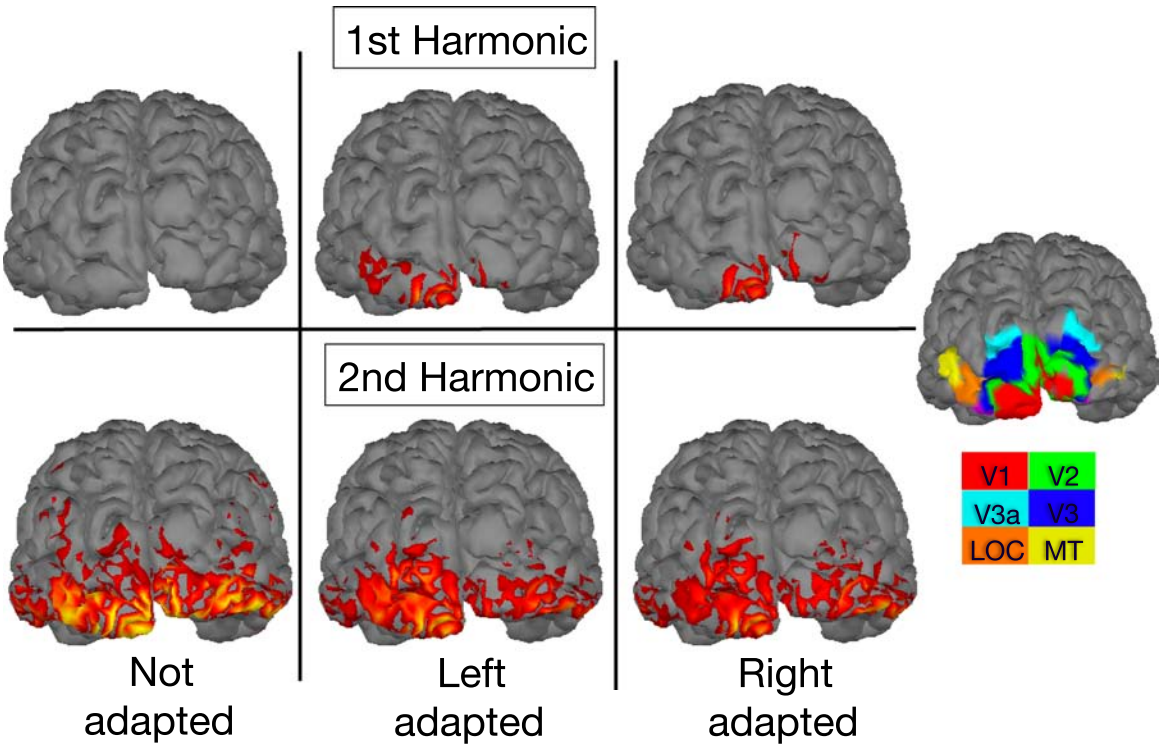

Figure 6. Cortical current density distributions for the same participant shown in Figure 4. The insert on the far right shows the visual ROIs from the fMRI mapping of visual areas for this participant. The top row shows the first harmonic, and the bottom row the second harmonic response. The order of the row and column data corresponds to that in Figure 4. The magnitude scaling is identical for all panels.

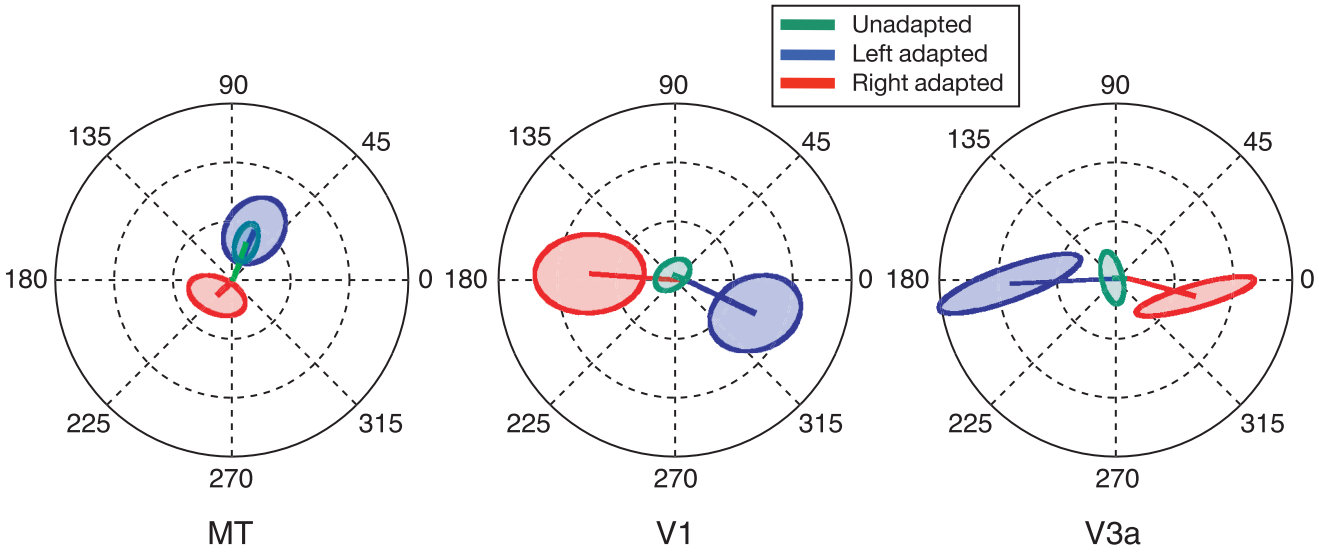

Figure 7. Group average first harmonic response from the MT, V1, and V3a ROIs. The length of the bar is the vector average of the response over all participants. The ellipse on the end of the bar is 1 standard error calculated from the group covariance.

The between-participant errors at the first harmonic are dominated by differences in response phase/latency that are present across participants. For our stimulus frequency of 9 Hz, a 180-degree phase shift corresponds to 55.5 ms of equivalent latency.

Degree of adaptation across ROI's

As an index of the degree to which each cortical ROI showed direction-specific adaptation, we calculated an adaptation index. For each participant, in each functionally mapped region, we calculated the total amplitude of the odd harmonics as a percent of the total summed amplitude of all harmonics. We then averaged the two adapted conditions and normalized this number by the nonadapted condition. This number quantifies the change in how much of the produced signal is directionally selective. A value greater then 1 means there is directionally selectivity, while a value of 1 means that the response does not change after adaptation. Figure 8 shows evidence of direction-specific adaptation across all visual areas, with the largest increases evident in dorsal V3, V3A, as well as in V1.

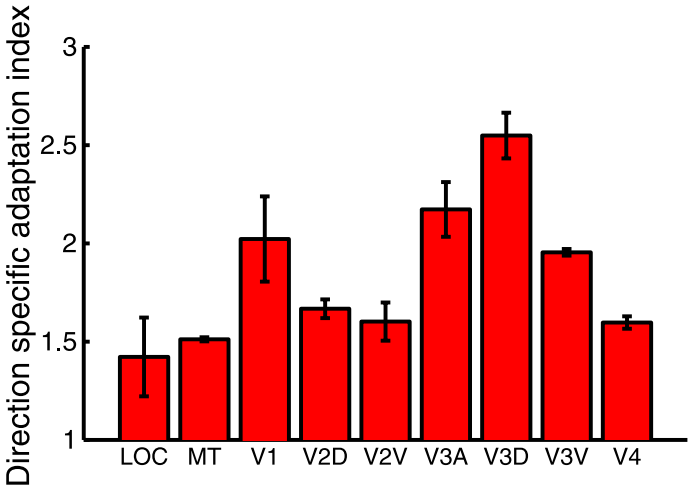

Figure 8. Direction-specific adaptation index across visual ROIs. The chart displays the fraction of odd harmonic amplitude in the adapted condition normalized by the nonadapted condition across the fMRI defined ROIs. The error bars are ±1 standard error across all participants.

Discussion

In the current literature, there is a disagreement between the observed distributions of direction selectivity from primate physiology and human fMRI. Physiologists have found individual neurons in many cortical areas that are direction selective, including V1 (Albright, 1984; Felleman & Van Essen, 1987; Kohn & Movshon, 2003; Orban et al., 1986). fMRI data have generally not shown clear evidence of direction selectivity in V1 (Ashida et al., 2007; Huk et al., 2001; Nishida et al., 2003). Using high-density EEG, a direct measure of neural response that may reflect cortical activity differently than the hemodynamic signal used in fMRI, we find evidence for direction selectivity in V1 and throughout retinotopic cortex.

Phase signature of directional selectivity in the SSVEP

We have described a new method for revealing the activity of populations of directionally selective neurons

using the visual evoked potential. The method improves over previous frequency domain measures (Heinrich & Bach, 2003; Tyler & Kaitz, 1977) by providing a distinctive temporal phase signature that is associated with the direction of adaptation. These frequency domain methods use the same test stimulus (an oscillating grating) for all conditions. Using the same stimulus to probe the system response avoids response effects due simply to the stimulus change. Other methods must also include conditions that control for adaptation effects that are not directionally specific (Heinrich & Bach, 2003; Hoffmann et al., 2001). The phase signature in our analysis finds directionally selective responses using a minimum of experimental conditions: one unadapted and two adaptation directions. A disadvantage of the frequency domain measures is that a direct assessment of the adaptability of a specific direction is not possible due to phase wrap-around effects inherent in the steady-state response. The frequency domain methods also provide more limited testing of the effects of adaptation on the population temporal impulse response.

Comparison with previous studies

Early fMRI studies found evidence for direction-specific motion aftereffects in cortical area MT (Culham et al., 1999; He, Cohen, & Hu, 1998; Tootell et al., 1995) that later studies showed were due to attentional modulation of the BOLD signal (Huk et al., 2001). The frequency domain VEP method is unlikely to suffer similar problems due to its use of a high temporal frequency test rather than a static test: attentional tracking is unlikely to be fast enough to modulate at 9 Hz, the frequency at which the VEP reads out the direction-specific population response.

Several fMRI studies have used direction-specific adaptation to study the cortical distribution of human motion mechanisms. Huk et al. (2001) found directionally selectivity throughout retinotopic cortex, with the strongest effects evident in V3a and hMT+. Nishida et al. (2003) also found directional effects in V3a and hMT+, with the largest effect in V3a. Nishida et al. did not find any directional effect in V1 for grating stimuli. However, second-order stimuli did show an effect in V1. Ashida et al. (2007) used both luminance and contrast modulated stimuli and found directionally specific effects in V3a and hMT+, with no evidence of activity in V1.

Similar to the fMRI studies, we find evidence for directionally selective response across our retinotopic ROI's, with the strongest effects occurring in the V3 and V3a ROIs. But we also find, in contrast to the fMRI studies, robust directional adaptation in our V1 ROI. Another difference is that the response measured from hMT+, while still exhibiting adaptation, does not show as great an effect as either the V1 or V3a ROIs.

One study recorded MEG responses to low contrast expanding/contracting rings after directional adaptation of (Amano et al., 2005). The authors found two peaks, M1 (latency from 150 to 200 ms) and M2 (latency from 200 to 300 ms), that each showed about a factor of 2 reduction of peak amplitude following same-direction adaptation. Dipole localization of these peaks found that both of these components could be fit with a dipole near the occipital pole/calcarine sulcus and/or a dipole in temporal–occipital cortex, depending on the subject. We find a proportionally greater direction-selective response change in V1 than MT, while Amano et al. (2005) find approximately equal effects in the putatively homologous locations. The difference in the amount of directionally specific reduction could be explained by the difference in stimuli—we used high contrast stimuli while Amano et al. used low contrast stimuli designed to preferentially activate MT responses because of the high contrast gain in MT.

Interpretation of indirect assays of population-level activity

Direction-specific neurons are intermingled at a scale that is too fine to be resolvable with the VEP. The synaptic activity of these populations is merged via volume conduction as the fields propagate to the scalp where the recording is made. The presence of direction-specific neurons could be inferred on the basis of biases in the distribution of the underlying neuronal population, but we find these biases to be too small to be used reliably—the response to left-right motion is even order prior to adaptation. fMRI has finer spatial resolution than the VEP, but even so, its native resolution is still too poor to isolate the activity of cells that are organized at the columnar level. Thus, other means, such as adaptation, must be used to detect direction-selective mechanisms.

Interpreting adaptation effects in both the VEP and the fMRI is complex. Bartels, Logothetis, and Moutoussis (2008) argued that if the BOLD signal primarily reflects pre-synaptic activity, the results from fMRI adaptation experiments might de-emphasize the actual site of adaptation and emphasize the locations receiving input from an adapted area. A similar argument could be made for the VEP, as its primary basis is also in synaptic activity (Nunez & Srinivasan, 2006). On this view, direction-selective adaptation could arise in an earlier area and appear on the inputs to a target area. If the VEP arose from this pre-synaptic activity, the second area would appear to be adaptable, when in fact it may not be, or in the limit, may not even have any direction-selective cells if the pre-synaptic activity does not contribute to direction-specific spiking activity. This scenario is implausible as it is unlikely that the VEP from any given cortical area is derived solely from pre-synaptic activity at

the input layer. The input to cortical visual areas arrives primarily in layer 4 (Nicholls, Martin, Wallace, & Kuffler, 1992), which is populated with small, spiny stellate cells whose spatial configuration does not lead to a measurable far-field potential (Nunez & Srinivasan, 2006). Rather, the surface-recorded VEP is generally believed to arise from pyramidal cells these are located outside of layer 4 (Nicholls et al., 1992). The VEP from a given area is thus likely to be dominated by local activity that is post-synaptic to the input layer. Feedback inputs onto pyramidal cells, however, could supply volume-conducted pre-synaptic activity that is not reflected in local spiking activity.

The ambiguity of the BOLD responses highlights the utility of using multiple neuroimaging techniques. In the current study, there exists an interesting disassociation between our EEG results and the fMRI results for both area V1 and area hMT+. The first is our finding of a robust effect in V1, where the fMRI studies find little or no change. The lack of finding in V1 is odd because it has been shown that most of the adaptation effects measured in MT in macaque can be attributed to changes in the responses of V1 (Kohn & Movshon, 2003). The argument that fMRI emphasizes synaptic input to an area in Bartels et al. (2008) could explain why the fMRI effect is most prominent in hMT+, which is downstream from adapted neurons in the V1 source. The apparent dissociation between our EEG results and fMRI may be because the EEG measures emphasize the activity from pyramidal cells, which carry the output of area V1 (Nicholls et al., 1992).

Conclusion

In conclusion, the present study has shown a new method for revealing directional selectivity from population responses. This method relies on finding odd harmonics that are 180 degrees phase shifted in the steady-state VEP response. Using this dynamic signature of direction selectivity, combined with high-density EEG and fMRI visual area mapping, we have shown that areas V1 (occipital pole) and V3/V3a (dorsal) locations contribute strongly to motion adaptation of the SSVEP response.

Acknowledgments

Commercial relationships: none.
Corresponding author: Justin Ales.
Email: ales@ski.org.
Address: The Smith-Kettlewell Eye Research Institute, 2318 Fillmore Street, San Francisco, CA 94115, USA.

References

Albright, T. D. (1984). Direction and orientation selectivity of neurons in visual area MT of the macaque. *Journal of Neurophysiology, 52,* 1106–1130. [PubMed]

Amano, K., Kuriki, I., & Takeda, T. (2005). Direction-specific adaptation of magnetic responses to motion onset. *Vision Research, 45,* 2533–2548. [PubMed]

Appelbaum, L. G., Wade, A. R., Vildavski, V. Y., Pettet, M. W., & Norcia, A. M. (2006). Cue-invariant networks for figure and background processing in human visual cortex. *Journal of Neuroscience, 26,* 11695–11708. [PubMed] [Article]

Ashida, H., Lingnau, A., Wall, M. B., & Smith, A. T. (2007). FMRI adaptation reveals separate mechanisms for first-order and second-order motion. *Journal of Neurophysiology, 97,* 1319–1325. [PubMed] [Article]

Bartels, A., Logothetis, N. K., & Moutoussis, K. (2008). fMRI and its interpretations: An illustration on directional selectivity in area V5/MT. *Trends Neurosciences, 31,* 444–453. [PubMed]

Brewer, A. A., Liu, J., Wade, A. R., & Wandell, B. A. (2005). Visual fields maps and stimulus selectivity in human ventral occipital cortex. *Nature Neuroscience, 8,* 1102–1109. [PubMed]

Bundo, M., Kaneoke, Y., Inao, S., Yoshida, J., Nakamura, A., & Kakigi, R. (2000). Human visual motion areas determined individually by magnetoencephalography and 3D magnetic resonance imaging. *Human Brain Mapping, 11,* 33–45. [PubMed]

Culham, J. C., Dukelow, S. P., Vilis, T., Hassard, F. A., Gati, J. S., Menon, R. S., et al. (1999). Recovery of fMRI activation in motion area MT following storage of the motion aftereffect. *Journal of Neurophysiology, 81,* 388–393. [PubMed] [Article]

Delon-Martin, C., Gobbele, R., Buchner, H., Haug, B. A., Antal, A., Darvas, F., et al. (2006). Temporal pattern of source activities evoked by different types of motion onset stimuli. *Neuroimage, 31,* 1567–1579. [PubMed]

DeYoe, E. A., Carman, G. J., Bandettini, P., Glickman, S., Wieser, J., Cox, R., et al. (1996). Mapping striate and extrastriate visual areas in human cerebral cortex. *Proceedings of the National Academy of Sciences of the United States of America, 93,* 2382–2386. [PubMed] [Article]

Felleman, D. J., & Van Essen, D. C. (1987). Receptive field properties of neurons in area V3 of macaque monkey extrastriate cortex. *Journal of Neurophysiology, 57,* 889–920. [PubMed]

Hamalainen, M. S., & Ilmoniemi, R. J. (1994). Interpreting magnetic fields of the brain: Minimum norm estimates. *Medical & Biological Engineering & Computing, 32,* 35–42. [PubMed]

Hamalainen, M. S., & Sarvas, J. (1989). Realistic conductivity geometry model of the human head for interpretation of neuromagnetic data. *IEEE Transactions on Biomedical Engineering, 36,* 165–171. [PubMed]

Handel, B., Lutzenberger, W., Thier, P., & Haarmeier, T. (2007). Opposite dependencies on visual motion coherence in human area MT+ and early visual cortex. *Cerebral Cortex, 17,* 1542–1549. [PubMed]

He, S., Cohen, E. R., & Hu, X. (1998). Close correlation between activity in brain area MT/V5 and the perception of a visual motion aftereffect. *Current Biology, 8,* 1215–1218. [PubMed]

Heinrich, S. P., & Bach, M. (2003). Adaptation characteristics of steady-state motion visual evoked potentials. *Clinical Neurophysiology, 114,* 1359–1366. [PubMed]

Hoffmann, M. B., Unsold, A. S., & Bach, M. (2001). Directional tuning of human motion adaptation as reflected by the motion VEP. *Vision Research, 41,* 2187–2194. [PubMed]

Holliday, I. E., & Meese, T. S. (2008). Optic flow in human vision: MEG reveals a foveo-fugal bias in V1, specialization for spiral space in hMSTs, and global motion sensitivity in the IPS. *Journal of Vision, 8*(10):17, 1–24, http://journalofvision.org/8/10/17/, doi:10.1167/8.10.17. [PubMed] [Article]

Huk, A. C., Ress, D., & Heeger, D. J. (2001). Neuronal basis of the motion aftereffect reconsidered. *Neuron, 32,* 161–172. [PubMed]

Huk, A. C., & Heeger, D. J. (2002). Pattern-motion responses in human visual cortex. *Nature Neuroscience, 5,* 72–75. [PubMed]

Jenkinson, M., Pechaud, M., & Smith, S. (2005). BET2: MR-based estimation of brain, skull and scalp surfaces. *In Eleventh Annual Meeting of the Organization for Human Brain Mapping.*

Kohn, A., & Movshon, J. A. (2003). Neuronal adaptation to visual motion in area MT of the macaque. *Neuron, 39,* 681–691. [PubMed]

Kourtzi, Z., & Kanwisher, N. (2000). Cortical regions involved in perceiving object shape. *Journal of Neuroscience, 20,* 3310–3318. [PubMed] [Article]

Lam, K., Kaneoke, Y., Gunji, A., Yamasaki, H., Matsumoto, E., Naito, T., et al. (2000). Magnetic response of human extrastriate cortex in the detection of coherent and incoherent motion. *Neuroscience, 97,* 1–10. [PubMed]

Nakamura, H., Kashii, S., Nagamine, T., Matsui, Y., Hashimoto, T., Honda, Y., et al. (2003). Human V5 demonstrated by magnetoencephalography using random dot kinematograms of different coherence levels. *Neuroscience Research, 46,* 423–433. [PubMed]

Nicholls, J. G., Martin, A. R., Wallace, B. G., & Kuffler, S. W. (1992). *From neuron to brain: A cellular and molecular approach to the function of the nervous system* (3rd ed.). Sunderland, Mass.: Sinauer Associates.

Nishida, S., Ledgeway, T., & Edwards, M. (1997). Dual multiple-scale processing for motion in the human visual system. *Vision Research, 37,* 2685–2698. [PubMed]

Nishida, S., Sasaki, Y., Murakami, I., Watanabe, T., & Tootell, R. B. (2003). Neuroimaging of direction-selective mechanisms for second-order motion. *Journal of Neurophysiology, 90,* 3242–3254. [PubMed] [Article]

Nunez, P. L., & Srinivasan, R. (2006). *Electric fields of the brain: The neurophysics of EEG* (2nd ed.). New York: Oxford University Press.

Orban, G. A., Kennedy, H., & Bullier, J. (1986). Velocity sensitivity and direction selectivity of neurons in areas V1 and V2 of the monkey: Influence of eccentricity. *Journal of Neurophysiology, 56,* 462–480. [PubMed]

Prieto, E. A., Barnikol, U. B., Soler, E. P., Dolan, K., Hesselmann, G., Mohlberg, H., et al. (2007). Timing of V1/V2 and V5+ activations during coherent motion of dots: An MEG study. *Neuroimage, 37,* 1384–1395. [PubMed]

Probst, T., Plendl, H., Paulus, W., Wist, E. R., & Scherg, M. (1993). Identification of the visual motion area (area V5) in the human brain by dipole source analysis. *Experimental Brain Research, 93,* 345–351. [PubMed]

Schellart, N. A., Trindade, M. J., Reits, D., Verbunt, J. P., & Spekreijse, H. (2004). Temporal and spatial congruence of components of motion-onset evoked responses investigated by whole-head magneto-electroencephalography. *Vision Research, 44,* 119–134. [PubMed]

Schor, C. M., & Levi, D. M. (1980). Direction selectivity for perceived motion in strabismic and anisometropoic amblyopia. *Investigative Ophthalmology & Visual Science, 19,* 1094–1104. [PubMed] [Article]

Sekuler, R. W., & Ganz, L. (1963). Aftereffect of seen motion with a stabilized retinal image. *Science, 139,* 419–420. [PubMed]

Smith, S. M. (2002). Fast robust automated brain extraction. *Human Brain Mapping, 17,* 143–155. [PubMed]

Smith, S. M., Jenkinson, M., Woolrich, M. W., Beckmann, C. F., Behrens, T. E., Johansen-Berg, H., et al. (2004).

Advances in functional and structural MR image analysis and implementation as FSL. *Neuroimage, 23,* Suppl. 1:S208–219. [PubMed]

Steiner, V., Blake, R., & Rose, D. (1994). Interocular transfer of expansion, rotation, and translation motion aftereffects. *Perception, 23,* 1197–1202. [PubMed]

Tootell, R. B., Reppas, J. B., Dale, A. M., Look, R. B., Sereno, M. I., Malach, R., et al. (1995). Visual motion aftereffect in human cortical area MT revealed by functional magnetic resonance imaging. *Nature, 375,* 139–141. [PubMed]

Tootell, R. B., & Hadjikhani, N. (2001). Where is 'dorsal V4' in human visual cortex? Retinotopic, topographic and functional evidence. *Cerebral Cortex, 11,* 298–311. [PubMed] [Article]

Tyler, C. W., & Kaitz, M. (1977). Movement adaptation in the visual evoked response. *Experimental Brain Research, 27,* 203–209. [PubMed]

Tyler, C. W., Baseler, H. A., Kontsevich, L. L., Likova, L. T., Wade, A. R., & Wandell, B. A. (2005). Predominantly extra-retinotopic cortical response to pattern symmetry. *Neuroimage, 24,* 306–314. [PubMed]

Victor, J. D., & Mast, J. (1991). A new statistic for steady-state evoked potentials. *Electroencephalography and Clinical Neurophysiology, 78,* 378–388. [PubMed]

von Pfostl, V., Stenbacka, L., Vanni, S., Parkkonen, L., Galletti, C., & Fattori, P. (2009). Motion sensitivity of human V6: A magnetoencephalography study. *Neuroimage, 45,* 1253–1256. [PubMed]

Wade, A. R., Brewer, A. A., Rieger, J. W., & Wandell, B. A. (2002). Functional measurements of human ventral occipital cortex: Retinotopy and colour. *Philosophical Transactions of the Royal Society of London B: Biological Sciences, 357,* 963–973. [PubMed] [Article]